



First principles study of structural, electronic and optical properties of indium gallium nitride arsenide lattice matched to gallium arsenide



Mohamed Issam Ziane ^{a,*}, Zouaoui Bensaad ^a, Tarik Ouahrani ^b,
Hamza Bennacer ^a

^a Applied Materials Laboratory, Research Center (CFTE), Sidi Bel Abbès Djillali Liabes University, 22000, Algeria

^b École Préparatoire en Sciences et Techniques, BP 165 R.P., 13000 Tlemcen, Algeria

ARTICLE INFO

Keywords:

Ab initio
InGaNAs
Lattice matched
Band structure
Optical properties

ABSTRACT

First principles calculations in the framework of the full-potential linearized augmented plane wave (FP-LAPW) scheme have been carried out. The dilute-nitride zinc blende ($\text{In}_x\text{Ga}_{1-x}\text{N}_y\text{As}_{1-y}$) was modeled at selected nitrogen compositions of $y=3.125\%$, 6.25% and 9.375% lattice matched to gallium arsenide (GaAs). We pay attention to the $\text{In}_x\text{Ga}_{1-x}\text{N}_y\text{As}_{1-y}$ alloy which can be perfectly lattice matched to the GaAs over its entire compositional range. In our study, this is achieved when a condition $y \sim 2.7x$ is maintained. The band structure calculations were performed with and without relaxation by using the generalized gradient approximation of Engel and Vosko (EV-GGA) as well as by the modified Becke–Johnson potential exchange (TB-mBJ). The action of the localized potential of subsisted nitrogen atoms was attributed to effect of relaxation. Increasing both indium and nitrogen compositions leads to decreasing energy band gap. In addition a band anti-crossing model (BAC) was also adopted to study the composition dependence of the direct band gap of quaternary alloys, building a bridge between their electronic and linear optical properties.

© 2014 Elsevier Ltd. All rights reserved.

1. Introduction

In recent years, III-V semiconductors have attracted both scientific and technological interest, due to their applications in the opto-electronic and technological effort. These semiconductor materials can crystallize in either the cubic zinc-blende phase (space group F43m) or the hexagonal wurtzite phase (space group P63mc). Gallium arsenide (GaAs) is one of the largest important semiconductor among III-V compounds, widely studied due to their significance in the technological application of

semiconductor industry. Another novel material system that has attracted considerable interest recently is the dilute nitride semiconductor. The latter is formed by alloying limited quantity of nitrogen into III-V semiconductor hosts [1]. Nitrogen containing GaAs has opened a new opportunity to largely extend the band gap engineering capabilities of III-V semiconductors materials [1]. It has been shown that the introduction of a small amount of nitrogen elements in the III-V hosts such as GaAs reduces the energy band gap by about 150 meV for only 1% of nitrogen [2]. Apart from GaNAs, the closing in the band gap has been remarked also in other ternary and quaternary alloys [3–8]. As explained by Elyukhin et al. [9], this reduction is mainly due to the transformation of the bonds after redistribution of the atoms in their lattice sites.

* Corresponding author. Tel.: +213 774884300.
E-mail address: issam1308@yahoo.fr (M.I. Ziane).

However, the closure of the electronic band gap induced by nitrogen (N) is then balanced by introducing an atom with high atomic radius such as indium (In) element [10]. An attractive material, which is expected to have significant advantages over the conventional III–V–N materials, is the quaternary InGaNAs alloy [11]. This alloy has received great attention [12–15] because of its direct band gap and relatively high mobilities. The InGaNAs quaternary alloys are the key materials for the fabrication of diverse electronic and optoelectronic components, especially in vertical cavity emitting source above 1.28 μm [16], high performance laser diodes emitting at 1.3 and 1.55 μm optical fiber windows [17,18], visible light emitting diodes (LEDs) [19], photodetector operating at 1.3 μm [20], avalanche photodiodes at 1.064 μm [21], heterojunctions bipolar transistors (HBTs) [22] and high efficiency solar cells [23]. Extensive investigations on InGaNAs lattice matched to GaAs have been reported by various experimental methods [24–26].

One of the most important tasks in the solid-state studies is to understand the atomic structure of a crystalline compound, in which the lattice constant is the key parameter. Therefore, an accurate knowledge of the nitrogen concentration effect on the electronic band gap energy of InGaNAs alloys is very important. Among recently published works on InGaNAs, we can find one theoretical study [27]. In their work M. Aslan and co-workers have calculated the structural and electronic properties of $\text{Ga}_{1-x}\text{In}_x\text{As}_{1-y}\text{N}_y$ quaternary alloys by using PWSCF code based on the plane-wave pseudopotential method within the local density approximation. They have examined the lattice constant and band gap energy for high In and N contents. In this work, we aim to present a theoretical prediction of the structural, electronic and optical properties of dilute-nitride zinc blende ($\text{In}_x\text{Ga}_{1-x}\text{N}_y\text{As}_{1-y}$) lattice matched to GaAs with nitrogen contents $y=3.125\%, 6.25\%$ and 9.375% by carrying out first principles calculation. Although the prediction of physical properties is the subject of our investigation, some aspects of the study of these properties remain controversial. Notably, ignorance persists regarding the scope of the interaction in the Brillouin Zone and hybridization states. This interaction is the source of the strong decrease of the band gap and the appearance of additional transition. Furthermore, the effects of nitrogen are assumed to be negligible at the band valence.

This article is organized as follows. In Section 2, we briefly describe the computational techniques used in this work. Results and discussions of our study will be presented in Section 3. Finally, a summary of this work is given in Section 4.

2. Computational details

The calculations presented in this paper have been performed within the framework of density functional theory (DFT) using the full potential linearized augmented plane wave (FP-LAPW) method as implemented in the Wien2k code [28]. This is a very accurate and efficient scheme to solve the Kohn–Sham equations [29]. The wave function basis used is mixed atomic functions and plane waves.

The exchange-correlation potential is treated within the WC-GGA. However, many calculations for solids [30] have showed that the GGA method constructed by Wu and Cohen in WC-GGA gives, at some extension, a good description of structural optimization. In order to develop and improve the FP-LAPW technique, a considerable effort has been devoted in the last 25 years to go beyond the standard approximations. In 1993 Engel and Vosko analyzed various versions of GGA exchange potentials and argued that, due to their particularly simple forms, GGAs are not able [31] to reproduce a good description of the band gap energy. In addition to the BAC model the generalized gradient approximation of Engel–Vosko (EV-GGA) [32] and the modified Becke–Johnson scheme (TB-mBJ), proposed recently by Tran and Blaha [33], were also used for electronic properties. It is worth reminding that these two latter approximations are not valid for the computations of the equilibrium structural parameters.

In order to simulate our quaternary alloys, we have used a $(2 \times 2 \times 2)$ supercell with 64 atoms. The crystal structures of $\text{In}_{0.093}\text{Ga}_{0.906}\text{N}_{0.031}\text{As}_{0.968}$, $\text{In}_{0.156}\text{Ga}_{0.843}\text{N}_{0.062}\text{As}_{0.937}$ and $\text{In}_{0.25}\text{Ga}_{0.75}\text{N}_{0.093}\text{As}_{0.906}$ quaternary alloys are shown in Fig. 1. The unit cell is divided into non-overlapping muffin-tin (MT) spheres around the atomic sites, and an interstitial region. From crystallography and under normal conditions, gallium arsenide (GaAs) and indium arsenide (InAs) have the B3 structure with space group F-43m [34] whereas gallium nitride (GaN) and indium nitride (InN) crystallize under normal conditions in the hexagonal wurtzite phase with the associated space group P63mc. The zinc blende structure (or sphalerite) for GaN and InN has been stabilized by epitaxial growth of the thin films on {011} crystal planes of cubic substrates [35]. In particular, works on zinc blende nitrides have attracted a great deal of theoretical attention due to their potential advantages they offer for optoelectronic applications compared to the commonly employed hexagonal nitrides [36]. The zinc blende structure is considered as a model system for all concerned materials used in this study. The simple cubic super-cell presented in Fig. 1 is constructed with 32 atoms of valency three (In/Ga) and thirty two pentavalent atoms (As/N) used to simulate the present material alloys. The muffin-tin radii R_{MT} were chosen equal to 2.20, 2.10, 1.76, and 2.15 a.u for In, Ga, N and As, respectively. The $R_{\text{MT}}K_{\max}$ parameter was taken equal to 7.0. To ensure the correctness of our calculations, we have taken $l_{\max}=10$ and $G_{\max}=14.0$. Also, the self-consistent calculations are considered to be converged when the total energy is stable within 0.1 mRy.

3. Results and discussion

3.1. Volume optimization

In order to calculate the ground state properties of ternary alloys $\text{In}_{0.093}\text{Ga}_{0.906}\text{As}$ and $\text{GaN}_{0.031}\text{As}_{0.968}$, and quaternary alloys $\text{In}_{0.093}\text{Ga}_{0.906}\text{N}_{0.031}\text{As}_{0.968}$, $\text{In}_{0.156}\text{Ga}_{0.843}\text{N}_{0.062}\text{As}_{0.937}$ and $\text{In}_{0.25}\text{Ga}_{0.75}\text{N}_{0.093}\text{As}_{0.906}$ alloys we must start from volume optimization of the constituent pure binaries. The non-

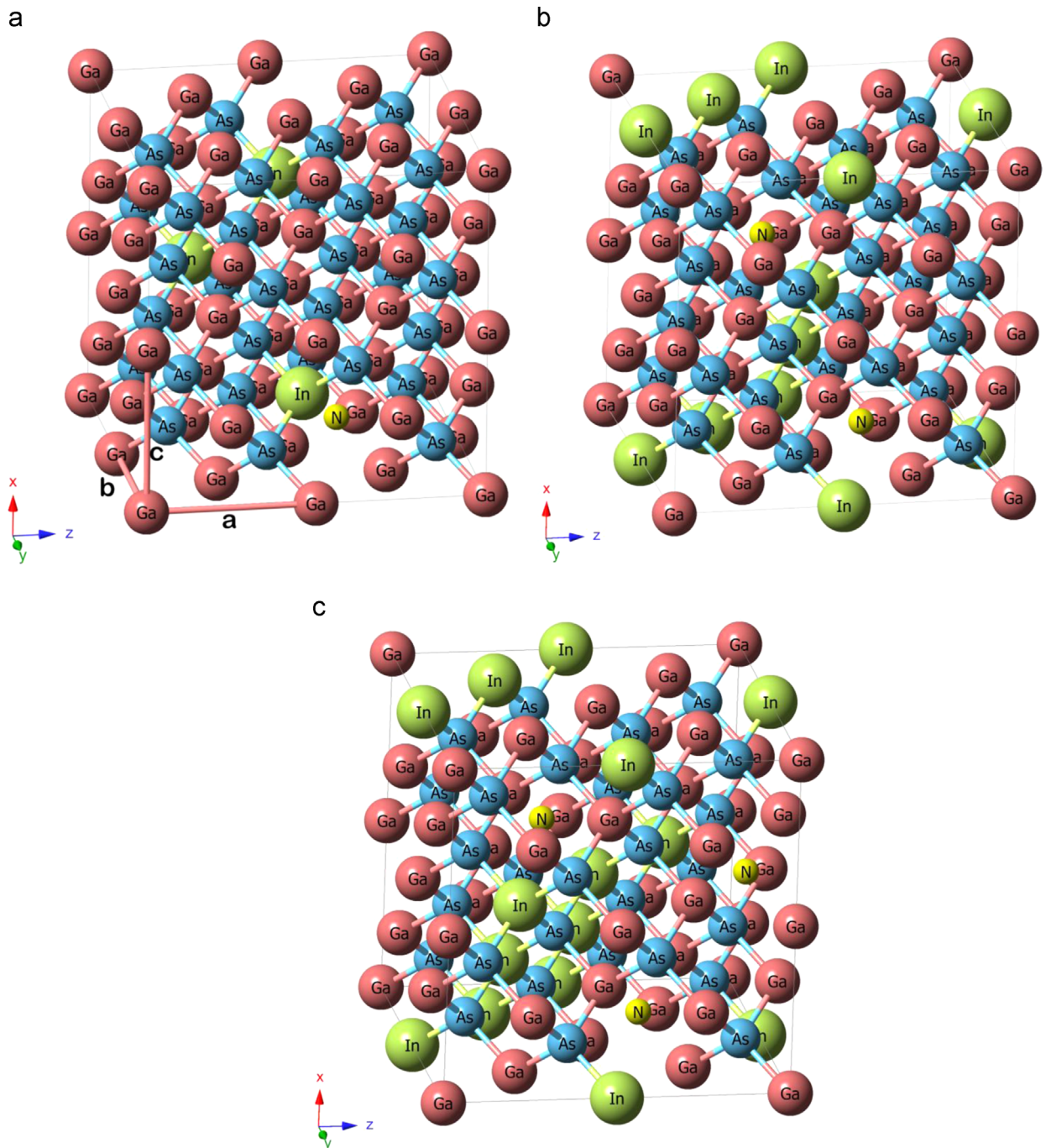


Fig. 1. Zinc blende structure for (a) $\text{In}_{0.093}\text{Ga}_{0.906}\text{N}_{0.031}\text{As}_{0.968}$, (b) $\text{In}_{0.156}\text{Ga}_{0.843}\text{N}_{0.062}\text{As}_{0.937}$ and (c) $\text{In}_{0.25}\text{Ga}_{0.75}\text{N}_{0.093}\text{As}_{0.906}$ (2ax2bx2c super-cell).

empirical density functional generalized gradient approximation of Wu and Cohen (WC-GGA) has emerged as one of the most important method for assessing the structural properties of solids. This form of GGA is able to provide significant improvement for lattice constants [30] over the most popular Perdew–Burke–Ernzerhof (PBE-GGA). One step forward to get insight into the physical properties of these materials is to perform a volume optimization starting from an experimental value. The optimized total energies of the system by using

WC-GGA formalism at different volumes were fitted to the Murnaghan's equation of states (EOS) [37].

We summarize our results with experimental and available theoretical values in Table 1. As is shown in this table, WC-GGA method has proven its value as an immensely powerful method [38] for predicting the lattice constant. It can be clearly seen that the calculated structural parameters of binary alloys are in excellent agreement with experimental values and other theoretical ones.

Table 1

The lattice constant a , bulk modulus B and its first pressure derivative B' of GaAs, GaN, InAs, InN, $\text{In}_x\text{Ga}_{1-x}\text{As}$, $\text{GaN}_y\text{As}_{1-y}$ and $\text{In}_x\text{Ga}_{1-x}\text{N}_y\text{As}_{1-y}$ compared to other available published results.

Material	$a(\text{\AA})$			$B(\text{GPa})$			B'	$\Delta a/a$
	Our results	Other works	Exp.	Our results	Other works	Exp.	Our results	in % from GaAs
GaAs	5.6640	5.666 ^a 5.609 ^b 5.551 ^c	5.64^d	68.977	69.60 ^a 75 ^b	77^d	4.62	0.00
GaN	4.5090	4.461 ^b 4.427 ^c 4.50 ^e	4.50^f	191.57	199 ^b 207.4 ^c	190^g	4.46	–
InAs	6.1065	5.956 ^c 6.191 ^b	6.058ⁱ	56.21	60 ^b 65.70 ^c	58^j	4.87	–
InN	4.9951	4.945 ^b 4.957 ^c	4.98^j	136.60	145 ^b 183.3 ^c	137^g	4.75	–
$\text{In}_{0.093}\text{Ga}_{0.906}\text{As}$	5.7123	–	–	71.179	–	–	3.20	–
$\text{GaN}_{0.031}\text{As}_{0.968}$	5.5913	–	–	85.148	–	–	4.25	–
$\text{In}_{0.093}\text{Ga}_{0.906}\text{N}_{0.031}\text{As}_{0.968}$	5.6365	–	–	83.939	–	–	3.80	0.48
$\text{In}_{0.156}\text{Ga}_{0.843}\text{N}_{0.062}\text{As}_{0.937}$	5.6426	–	–	83.777	–	–	4.25	0.37
$\text{In}_{0.25}\text{Ga}_{0.75}\text{N}_{0.093}\text{As}_{0.906}$	5.6675	–	–	86.240	–	–	4.34	0.061

^a Ref. [42].

^b Ref. [43].

^c Ref. [27].

^d Ref. [44].

^e Ref. [45].

^f Ref. [46].

^g Ref. [47].

^h Ref. [48].

ⁱ Ref. [49].

^j Ref. [50].

Let us now turn to predict the structural properties of the two ternary alloys formed by the binary zinc blend compounds presented above. By performing self-consistent calculations, the structural properties *i.e.* lattice constant, bulk modulus and its first pressure derivative of the ternary alloys such as $\text{In}_x\text{Ga}_{1-x}\text{As}$ and $\text{GaN}_y\text{As}_{1-y}$ have been obtained at $x=0.093$ and $y=0.031$.

According to Vegard's law [39] the lattice constant for the alloys of the form can be derived from pure binaries parameter:

$$\left\{ \begin{array}{l} a_{\text{In}_x\text{Ga}_{1-x}\text{As}} = xa_{\text{InAs}} + (1-x)a_{\text{GaAs}} \\ a_{\text{GaN}_y\text{As}_{1-y}} = ya_{\text{GaN}} + (1-y)a_{\text{GaAs}} \end{array} \right. \quad (1)$$

In Table 1, we summarize the computed equilibrium lattice constant a , bulk modulus B and its first derivative B' which have been obtained from the full optimization of the total energy by using the lattice constants calculated using Eq. (1) for two composition parameters $x=0.093$ and $y=0.031$. From this result we can observe that the lattice constant in $\text{In}_{0.093}\text{Ga}_{0.906}\text{As}$ alloy increases when a few percent of indium atoms is added to the host semiconductor GaAs, while for the same host semiconductor (GaAs), the replacement of one arsenic atom by one isoelectronic nitrogen atom results in reduction of the lattice parameter compared to that of GaAs. The lattice constants a for GaAs and $\text{In}_{0.093}\text{Ga}_{0.906}\text{As}$ are found to be around 5.664 and 5.712 Å, while for $\text{GaN}_{0.031}\text{As}_{0.968}$ the latter is found to be around 5.591 Å. It should be noted that we can establish a relationship between the substituted atom size defined by its atomic radius and the dimensions of the lattice crystal (lattice parameter).

Quaternary alloy of composition $\text{In}_x\text{Ga}_{1-x}\text{N}_y\text{As}_{1-y}$ may be thought to be formed out of four binary compounds [40]: InN, InAs, GaN and GaAs, with composition ratios

given respectively by xy , $x(1-y)$, $(1-x)y$ and $(1-x)(1-y)$:

$$a_{\text{In}_x\text{Ga}_{1-x}\text{N}_y\text{As}_{1-y}} = xy a_{\text{InN}} + (1-x)y a_{\text{GaN}} + x(1-y) a_{\text{InAs}} + (1-x)(1-y) a_{\text{GaAs}} \quad (2)$$

The lattice constants, bulk modulus and first pressure derivatives of the bulk modulus of $\text{In}_x\text{Ga}_{1-x}\text{N}_y\text{As}_{1-y}$ for selected values of x and y are calculated and listed in Table 1. To the best of our knowledge, there are no experimental or theoretical values for the structural properties of $\text{In}_x\text{Ga}_{1-x}\text{N}_y\text{As}_{1-y}$ alloys in these configurations. Our calculated lattice constant of $\text{In}_{0.093}\text{Ga}_{0.906}\text{N}_{0.031}\text{As}_{0.968}$, $\text{In}_{0.156}\text{Ga}_{0.843}\text{N}_{0.062}\text{As}_{0.937}$ and $\text{In}_{0.25}\text{Ga}_{0.75}\text{N}_{0.093}\text{As}_{0.906}$ obtained using WC-GGA functional are 5.636, 5.642 and 5.667 Å, respectively. We notice a small mismatch (less than 0.48%) between the two semiconductors of InGaNAs/GaAs structures. The lattice mismatch is given by [41]:

$$\frac{\Delta a}{a_{\text{GaAs}}} = \frac{a_{\text{InGaNAs}} - a_{\text{GaAs}}}{a_{\text{GaAs}}} 100\% \quad (3)$$

If we take the quaternary $\text{In}_{0.093}\text{Ga}_{0.906}\text{N}_{0.031}\text{As}_{0.968}$ as an example, the host material is GaAs with a lattice parameter of 5.664 Å. The incorporation of 9.375% of indium ($\text{In}_{0.093}\text{Ga}_{0.906}\text{As}$) increases the lattice parameter to a value of 5.71 Å. The increase in the lattice parameter is justified by the fact that the atomic size of indium is larger than those of Ga and As atoms. Thereafter, a reduction of lattice parameter of about 5.635 Å results from the substitution of one arsenic atom by one highly electronegative and isoelectronic nitrogen atom in $\text{In}_{0.093}\text{Ga}_{0.906}\text{As}$ alloy. The lattice parameter here is influenced by the increase or decrease of the In and N atoms. To shed more light on this behavior, we have computed and gathered in Fig. 2 the dependence of the lattice constant on the concentration of In and N substituent. This allows us to see the effect of such concentration on the structural parameters.

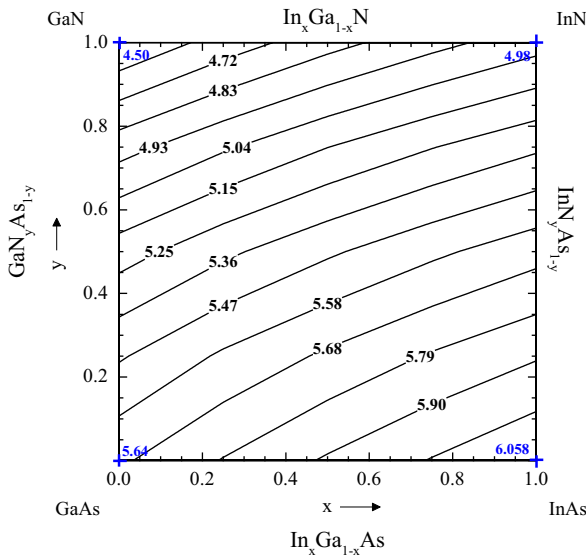


Fig. 2. Calculated (a) lattice constant contour lines for $\text{In}_x\text{Ga}_{1-x}\text{N}_y\text{As}_{1-y}$ with WC-GGA. The experiment lattice constant values of GaAs, InAs, GaN and InN are indicated (+ symbols). Lattice constant are labeled in Å.

In fact, Fig. 2 shows the calculated lattice constant contour lines for $\text{In}_x\text{Ga}_{1-x}\text{N}_y\text{As}_{1-y}$ alloy while it is clearly visible that the lattice parameter increases with increasing In composition and decreases with increasing N atoms.

Table 1 shows that lattice constant increases and, therefore, lattice mismatch decreases with increasing x and y contents in $\text{In}_x\text{Ga}_{1-x}\text{N}_y\text{As}_{1-y}$. We have paid particular attention to the choice of the quaternary configurations to mimic as closely as possible the $\text{InGaNAs}/\text{GaAs}$ structure. This plays an important role in achieving a good heterostructure with a good lattice matching of the two constituent materials. The calculated lattice matching expression for quaternary compound $\text{In}_x\text{Ga}_{1-x}\text{N}_y\text{As}_{1-y}$ on GaAs substrate is

$$y = \frac{0.442x}{1.15 - 0.043x} \quad (4)$$

3.2. Band structure and density of charge

The band structures of the quaternary materials under study were calculated using three approximations: WC-GGA, EV-GGA, TB-mBJ, plus the band anti-crossing model (BAC). Many calculations in the literature have demonstrated that the simplest conventional approaches such as LDA and GGA are plagued by the problem of large band gap errors in semiconductors [38] and, hence, fail to correctly describe the electronic band structure. Thus, to overcome this situation, the alternative form of GGA proposed by Engel and Vosko (EV-GGA) and the modified Becke-Johnson potential (TB-mBJ) developed by Tran and Blaha were used in this study.

A final remark, suggested by a referee, has to do with the contribution coming from structural and ionic relaxation. To this end, all atoms are allowed to relax until the force on each one is minimized. Note that relaxing such a system is

computationally expensive. In Table 2, we present the atomic geometric arrangements of two types of structure: the system with fixed and relaxed structural parameters. The computed band structures with no relaxed structural parameters for quaternary alloys performed by TB-mBJ approach for the calculated equilibrium lattice constants along the high symmetry directions are shown in Figs. 3 and 4. The Fermi level in Fig. 4 is set to zero and indicated by the horizontal red solid line. From our first analysis, we deduce that all quaternary alloys are direct band gap materials semiconductors, the valence band maximum and the conduction band minimum being situated at the Γ point. The obtained results of binary, ternary and quaternary compounds within WC-GGA, EV-GGA, TB-mBJ and BAC model are gathered in Table 3. Besides our own results, Table 3 includes also previous experimental and theoretical published results from other research works. Large discrepancies between our WC-GGA results and the experimental values for binary compounds are found; energy gap is underestimated by about 77% and 49%, respectively, for GaAs and GaN, whereas for InX ($X=\text{As}, \text{N}$) WC-GGA practically gives a zero band gap. As expected, this approximation leads always to a strong underestimation of band gaps. The EV-GGA bandgap values show an intermediate error of 36.05%, 28.5%, 72.18% and 83.5% compared to the experimental results for GaAs, GaN, InAs and InN, respectively. These differences are minimized for the Tran and Blaha-mBJ functional [33].

In order to understand the discrepancy between relaxed and un-relaxed quaternary structures, let us focus on the electronic band gap calculated of these two geometries within the three approximations. Comparison between the calculated band gap energy for the fixed and relaxed atomic postions obtained by the three approximations gives significantly different results. It is found from Table 3 that the TB-mBJ band gap for $\text{In}_{0.093}\text{Ga}_{0.906}\text{N}_{0.031}\text{As}_{0.968}$ calculated before and after relaxation of 1.268 and 0.819 eV is overestimated by about 0.17 and 0.27 eV, respectively, compared to the experimental value of 1.089 eV measured by Geisz et al. [61] on the basis of X-ray data for 8% indium composition. The incorporation of one N atom into $\text{In}_{0.093}\text{Ga}_{0.906}\text{As}$ leads to a reduction of the band gap in the un-relaxed $\text{In}_{0.093}\text{Ga}_{0.906}\text{N}_{0.031}\text{As}_{0.968}$ quaternary alloy by about 120 meV.

For the same nitrogen content added to the host semiconductor matrix, a small band gap energy reduction in $\text{In}_x\text{Ga}_{1-x}\text{N}_y\text{As}_{1-y}$ than in $\text{GaN}_y\text{As}_{1-y}$ has been explicitly observed by Morkoç [35].

The alloying effects in III-V dilute nitrides [51] and other highly mismatched alloys have been described in terms of two interacting energy levels band anti-crossing model [52]. The band gap energy of InGaNAs according to this model corresponds to the lower eigenvalue of the Hamiltonian, E , derived from

$$E_{\pm} = \frac{1}{2} \left[E_N + E_M \pm \sqrt{(E_N - E_M)^2 + 4(C_{MN})^2 y} \right] \quad (5)$$

Here, E_+ corresponds to the energy of the optical transition between the valence band and the second conduction subband. E_N is the energy of the N localized level introduced by the more electronegative isoelectronic atoms and E_M

Table 2

In and N atomic relaxed and unrelaxed positions in $\text{In}_x\text{Ga}_{1-x}\text{N}_y\text{As}_{1-y}$ semiconductors for the three compositions alloys.

Materials	In atom positions (x,y,z)		N atom positions (x,y,z)	
	Unrelaxed	Relaxed	Unrelaxed	Relaxed
QA1	$\text{In}_1(0.00, 0.50, 0.00)$	$\text{In}_1(0.999, 0.499, 0.000)$	$\text{N}(0.125, 0.625, 0.625)$	$\text{N}(0.1249, 0.6249, 0.6249)$
	$\text{In}_2(0.00, 0.00, 0.50)$	$\text{In}_2(0.999, 0.000, 0.499)$		
	$\text{In}_3(0.50, 0.50, 0.50)$	$\text{In}_3(0.500, 0.499, 0.499)$		
QA2	$\text{In}_1(0.00, 0.50, 0.00)$	$\text{In}_1(0.997, 0.501, 0.00)$	$\text{N}_1(0.125, 0.625, 0.625)$	$\text{N}_1(0.1246, 0.6263, 0.6260)$
	$\text{In}_2(0.00, 0.00, 0.50)$	$\text{In}_2(0.995, 0.998, 0.50)$	$\text{N}_2(0.625, 0.375, 0.375)$	$\text{N}_2(0.625, 0.375, 0.375)$
	$\text{In}_3(0.50, 0.50, 0.50)$	$\text{In}_3(0.516, 0.484, 0.482)$		
	$\text{In}_4(0.25, 0.25, 0.50)$	$\text{In}_4(0.252, 0.249, 0.501)$		
	$\text{In}_5(0.00, 0.25, 0.25)$	$\text{In}_5(0.001, 0.252, 0.250)$		
QA3	$\text{In}_1(0.00, 0.50, 0.00)$	$\text{In}_1(0.992, 0.504, 0.997)$	$\text{N}_1(0.125, 0.625, 0.625)$	$\text{N}_1(0.1229, 0.6287, 0.6287)$
	$\text{In}_2(0.00, 0.00, 0.50)$	$\text{In}_2(0.992, 0.997, 0.504)$	$\text{N}_2(0.625, 0.375, 0.375)$	$\text{N}_2(0.6322, 0.3677, 0.3677)$
	$\text{In}_3(0.50, 0.50, 0.50)$	$\text{In}_3(0.519, 0.485, 0.485)$	$\text{N}_3(0.625, 0.875, 0.875)$	$\text{N}_3(0.6247, 0.8753, 0.8753)$
	$\text{In}_4(0.25, 0.25, 0.50)$	$\text{In}_4(0.251, 0.248, 0.499)$		
	$\text{In}_5(0.25, 0.50, 0.25)$	$\text{In}_5(0.251, 0.499, 0.248)$		
	$\text{In}_6(0.00, 0.25, 0.25)$	$\text{In}_6(0.998, 0.249, 0.249)$		
	$\text{In}_7(0.50, 0.75, 0.25)$	$\text{In}_7(0.499, 0.751, 0.250)$		
	$\text{In}_8(0.50, 0.25, 0.75)$	$\text{In}_8(0.499, 0.250, 0.751)$		

QA1: $\text{In}_{0.093}\text{Ga}_{0.906}\text{N}_{0.031}\text{As}_{0.968}$.

QA2: $\text{In}_{0.156}\text{Ga}_{0.843}\text{N}_{0.062}\text{As}_{0.937}$.

QA3: $\text{In}_{0.25}\text{Ga}_{0.75}\text{N}_{0.093}\text{As}_{0.906}$.

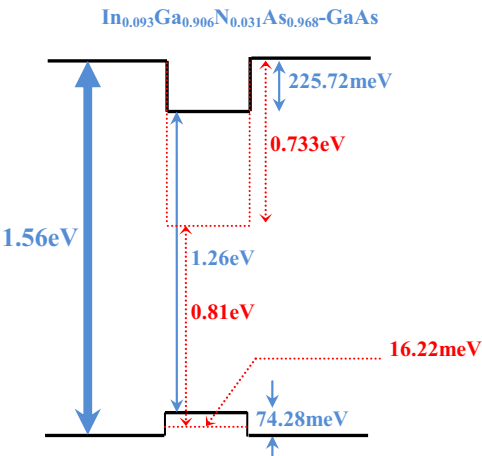


Fig. 3. Relaxed (red dotted line) and un-relaxed (black solid line) $\text{InGaNAs}/\text{GaAs}$ structure.

represents the extended states of the semiconductor matrix given, respectively, by the following equations [53–55]

$$E_N = 1.65(1-x) + 1.44x - 0.38x(1-x) \quad (6)$$

$$E_M = E_0 - 1.55y \quad (7)$$

where x and y are the In and N mole fractions and E_0 is the energy of the host semiconductor in the absence of nitrogen. The energy versus composition equation that gives the variation of the band gap E_0 is here [54]

$$E_{\text{In}_x\text{Ga}_{1-x}\text{As}} = 1.512 - 1.337x + 0.27x^2 \quad (8)$$

The matrix element coupling the localized and extended states C_{MN} in Eq. (5) is taken to be 2.7 eV [55].

The band gap energy of $\text{In}_x\text{Ga}_{1-x}\text{N}_y\text{As}_{1-y}$ alloys with concentrations $(x,y)=(3\% \text{ and } 1\%), (5\% \text{ and } 2\%), \text{ and } (8\%$

and 3%) obtained from BAC model calculations are 0.974, 0.692 and 0.427 eV, respectively, as shown in Table 3. The BAC model of Shan et al. [52] is regarded as a reasonably accurate method for predicting the fundamental band gap of $\text{In}_x\text{Ga}_{1-x}\text{N}_y\text{As}_{1-y}$ alloy systems for small nitrogen concentrations. Comparison with previous experimental and theoretical results reveals that our BAC band gap of 0.974 eV for $\text{In}_{0.093}\text{Ga}_{0.906}\text{N}_{0.031}\text{As}_{0.968}$ is in agreement with the result calculated by Turcotte et al. (1.10 eV) [60] and the experimental value (1.08 eV) of Ref. [61]. It may be also noted here that, for the same quaternary alloy, the EV-GGA calculation with and without relaxation is underestimated compared to the BAC result by about 15% and 20%, respectively. However, the TB-mBJ calculation is overestimated by about 30% without relaxation, and underestimated by about 15% by including the relaxation effect. We observe a decreasing band gap of the quaternary alloys under study as x and y concentrations increase.

Band gap of semiconductors is strongly influenced by the bond lengths and lattice parameter a , in other words by the size of the constituents atoms of the crystal. As mentioned in the previous subsection, the variation in lattice parameter is related to radius of the particle added in the host semiconductor. As demonstrated by various theoretical and experimental works, the band gap decreases with increasing atomic size of the anion element, i.e. in inverse relation to lattice constant a . To clarify this point, we have presented in Fig. 5 the calculated mBJ bandgap contour lines of $\text{In}_x\text{Ga}_{1-x}\text{N}_y\text{As}_{1-y}$ alloy as a function of x and y concentrations. As shown in Fig. 5, the bandgap of the quaternary alloys seems to decrease with the increase of indium content. On the other hand, when the nitrogen substituent concentration increases, the bandgap value increases. The situation is the same with the incorporation of the N content into the $\text{In}_x\text{Ga}_{1-x}\text{As}$ as in GaAs. According to Shan et al. [52], this can be explained by

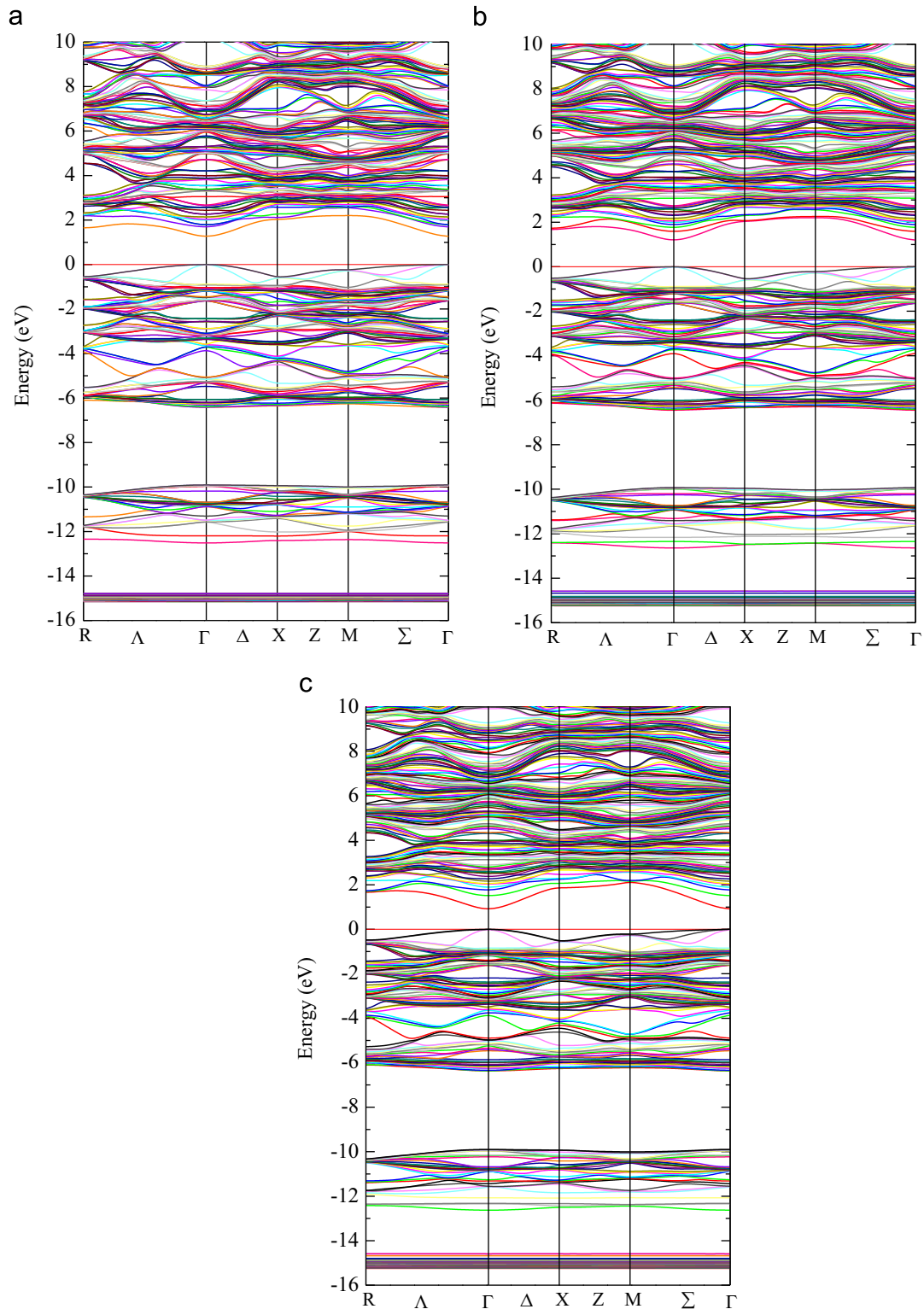


Fig. 4. No relaxed band structure within TB-mBJ at the equilibrium lattice constant for (a) $\text{In}_{0.093}\text{Ga}_{0.906}\text{N}_{0.031}\text{As}_{0.968}$ (b) $\text{In}_{0.156}\text{Ga}_{0.843}\text{N}_{0.062}\text{As}_{0.937}$ and (c) $\text{In}_{0.25}\text{Ga}_{0.75}\text{N}_{0.093}\text{As}_{0.906}$.

the strong interaction between the extended states of the conduction band of the host semiconductor such as InGaAs and the localized resonant states of the nitrogen N. The

relaxation of surrounding ions is important in determining the off-center instability of the substituted atom. Thus, in order to avoid the ambiguity related to the effect of

Table 3

Band gap E_g for GaAs, GaN, InAs, InN, InGaAs, GaNAs and InGaNAs calculated with WC-GGA, EV-GGA, TB-mBJ and BAC model compared with other results.

Material	E_g (eV)					Exp.
	WC-GGA	EV-GGA	TB-mBJ	BAC	Other works	
GaAs	0.344	0.972	1.565	—	0.336 ^{a,b} 1.03 ^c 1.55 ^d 1.64 ^e	1.52^e
GaN	1.645	2.288	2.948	—	1.645 ^a 2.34 ^f 2.81 ^c 2.89 ^d	3.2^e
InAs	0.00	0.116	0.508	—	0.00 ^{c,g} 0.34 ^g 0.40 ^c 0.57 ^d	0.417^h
InN	0.00	0.113	0.660	—	0.00 ⁱ 0.081 ^f 0.142 ^f	0.7^f
$\text{In}_{0.093}\text{Ga}_{0.906}\text{As}$	0.170	0.783	1.382	—	1.426 ^j	—
$\text{GaN}_{0.031}\text{As}_{0.968}$	0.415	1.034	1.445	1.070	—	—
$\text{In}_{0.093}\text{Ga}_{0.906}\text{N}_{0.031}\text{As}_{0.968}$				0.974	1.101 ^j	1.089^k
un-relaxed alloy	0.174	0.778	1.268			
relaxed alloy	0.000	0.389	0.819			
$\text{In}_{0.156}\text{Ga}_{0.843}\text{N}_{0.062}\text{As}_{0.937}$				0.692	—	—
un-relaxed alloy	0.125	0.720	1.202			
relaxed alloy	0.000	0.224	0.640			
$\text{In}_{0.25}\text{Ga}_{0.75}\text{N}_{0.093}\text{As}_{0.906}$				0.427	—	—
un-relaxed alloy	0.000	0.453	0.913			
relaxed alloy	0.000	0.000	0.113			

^a Ref. [56].

^b Ref. [42].

^c Ref. [50].

^d Ref. [57].

^e Ref. [33].

^f Ref. [58].

^g Ref. [48].

^h Ref. [46].

ⁱ Ref. [59].

^j Ref. [60].

^k Ref. [61].

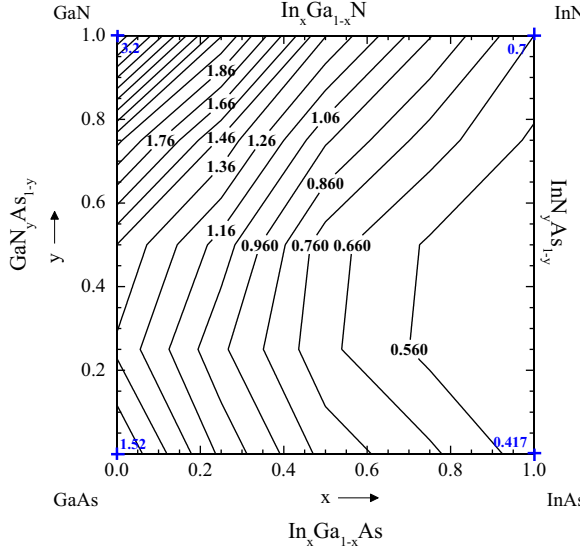


Fig. 5. Calculated mBJ bandgap contour lines for $\text{In}_x\text{Ga}_{1-x}\text{N}_y\text{As}_{1-y}$. The experiment band gaps for InN, GaN, InAs and GaAs are indicated (+ symbols). All values are labeled in eV.

substituted nitrogen atom, the investigated super-cells have been relaxed. Taking advantage of the constrained relaxation of internal coordinates we have plotted the three atomic configurations of quaternary alloys in Fig. 6, where non-negligible inwards movements towards the substituted nitrogen are shown. This result indicates a significant coupling between the off-center N and its host. The

inclusion of this atom affects the first and second nearest-neighbor. We should point out here that the bonding nature of the super-cell is weakly affected (see Table 4).

The effect of atomic configuration is also showed in Fig. 7. In fact, the relaxation is very localized about the nitrogen substituted site and primarily involves motion of the two adjacent atoms to the substituted lattice site.

The analysis of bonding interaction from the charge density distribution $\rho(r)$ alone may mislead the identification of the nature of chemical bonding. To overcome this, we have exploited the topological feature of $\rho(r)$ (more detail can be found in Ref [62]). The principle of this method is based on the recursive division of the irreducible wedge of the Wigner–Seitz polyhedron of the Bravais lattice and the minimization of $|\rho(r)|$ within the edges, surfaces and interiors of the resulting tetrahedral. The most significant and comprehensive form that we have found is depicting the attraction basins for each nuclei, displayed in Fig. 8.

We can determine a single parameter describing the global charge transferred by averaging the ratios between the nominal (topological) charges ($Q(\Omega)$) and the nominal oxidation states ($\text{OS}(\Omega)$):

$$\alpha = \frac{1}{N} \sum_1^N \frac{Q(\Omega)}{\text{OS}(\Omega)} \quad (9)$$

Table 4 provides a rough picture of bonding behavior of our quaternary alloys. The inclusion of the nitrogen atoms leads to decreasing ionic character and, therefore, a decrease of the energy gap value. However, we can clearly see that the relaxation effect is not felt considerably

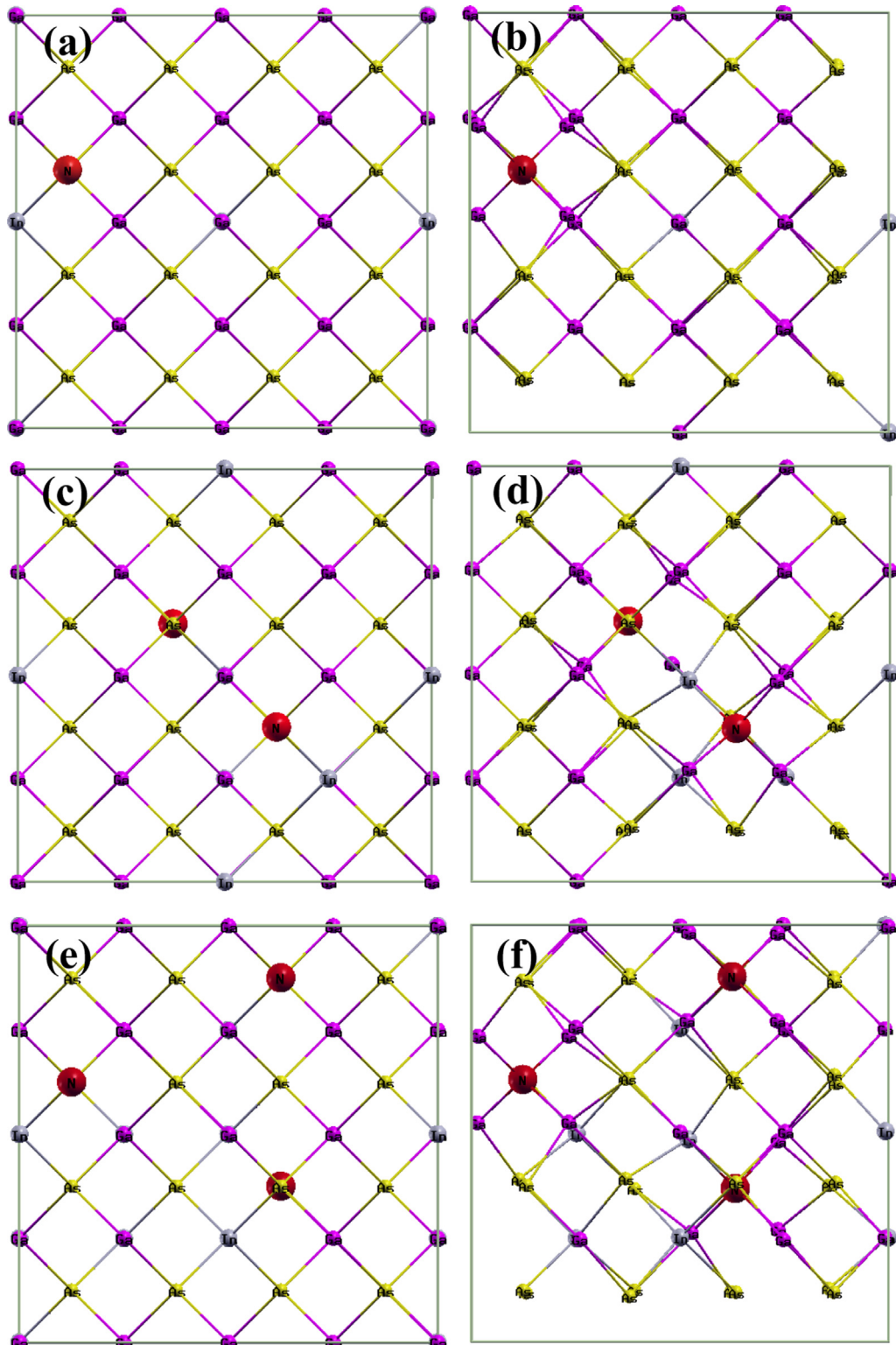


Fig. 6. 2D representatitif plot of the effect of substituted nitrogen atom on the super-cell, (a), (c), (e) for no relaxed structures and (b), (d), (f) for relaxed ones. The plot shows the potential localization of the N atom, affecting the first and second nearest-neighbor.

on the bonding behavior (the nitrogen becomes too small to strongly influence the host). Also, different configurations of the inclusion of the N atom of Fig. 9 give a very

close degree of ionicity: this allows us to conclude that the location of the N atom has a slight influence on the bonding properties of $\text{In}_x\text{Ga}_{1-x}\text{N}_y\text{As}_{1-y}$ alloys.

Therefore, due to the deformation of the bands by the action of the localized potential of nitrogen, a remarkable decrease of the band gap with the incorporation of N atom is established (practically more than 50%, see Table 3).

Table 4

Ionicity for $\text{In}_{0.093}\text{Ga}_{0.906}\text{N}_{0.031}\text{As}_{0.968}$, $\text{In}_{0.156}\text{Ga}_{0.843}\text{N}_{0.062}\text{As}_{0.937}$ and $\text{In}_{0.25}\text{Ga}_{0.75}\text{N}_{0.093}\text{As}_{0.906}$.

Material	Ionicity degree (%)	
	Relaxed structure	No relaxed structure
$\text{In}_{0.093}\text{Ga}_{0.906}\text{N}_{0.031}\text{As}_{0.968}$	89.47023	89.39684
$\text{In}_{0.156}\text{Ga}_{0.843}\text{N}_{0.062}\text{As}_{0.937}$	76.82228	76.83159
$\text{In}_{0.25}\text{Ga}_{0.75}\text{N}_{0.093}\text{As}_{0.906}$	59.49765	50.18033

The incorporation of this latter breaks the symmetry of the host material. Although the nitrogen has the same valence as that of the substitute atoms, the difference in electronegativity of the N compared to the indium implies that this anion becomes electrically active. The first conduction band is divided into two conduction subbands, where the upper one is formed of single characteristic diluted nitrides. In addition, the two formed sub-bands are highly non-parabolic. However, limiting our focus around the critical point Γ , it is listed that the effective mass in the case of diluted nitrogen becomes much larger (about 2-fold) than in GaAs as the nitrogen is incorporated [63].

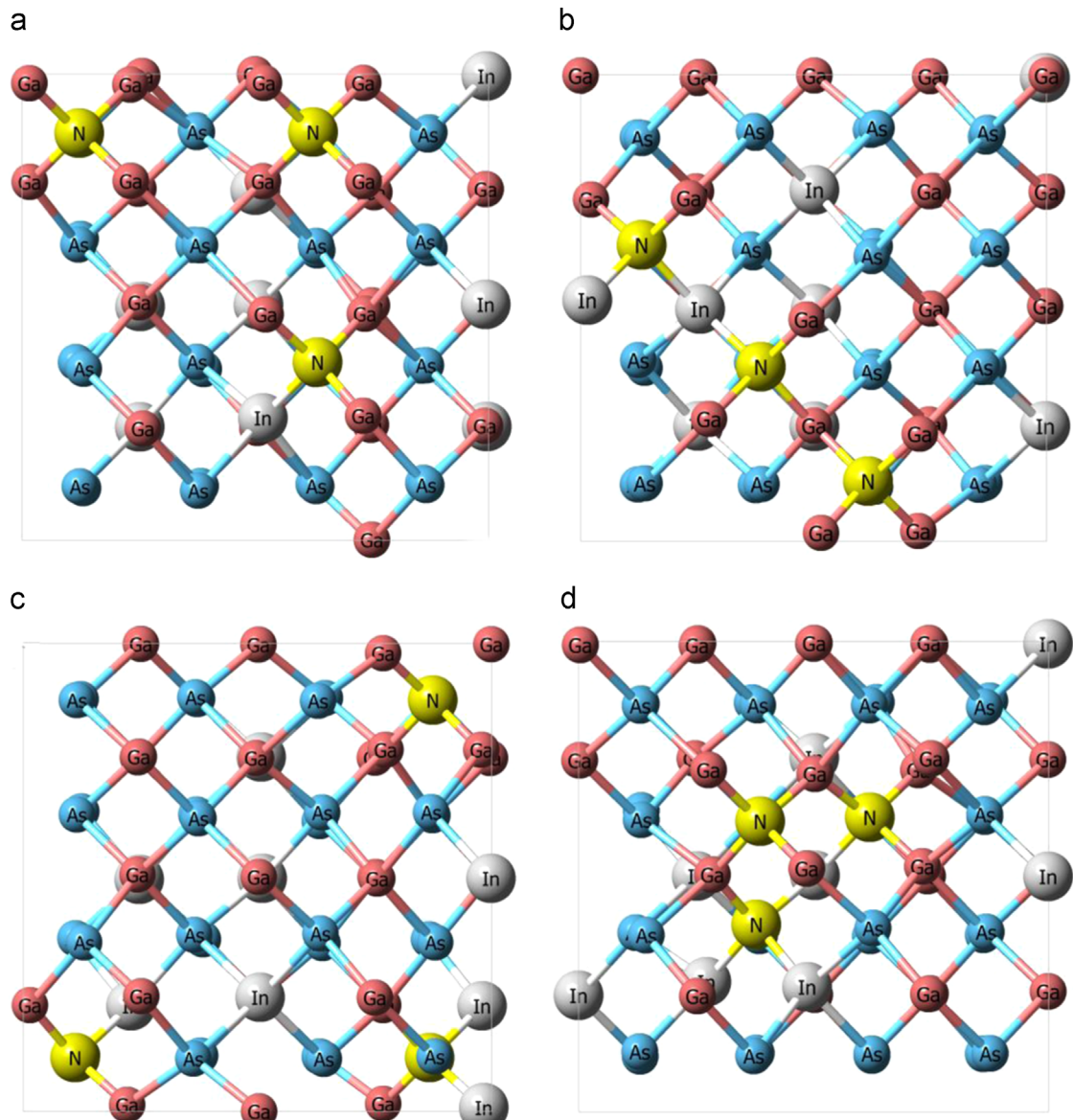


Fig. 7. The effect of atomic configuration in the $\text{In}_{0.25}\text{Ga}_{0.75}\text{N}_{0.093}\text{As}_{0.906}$ quaternary alloy.

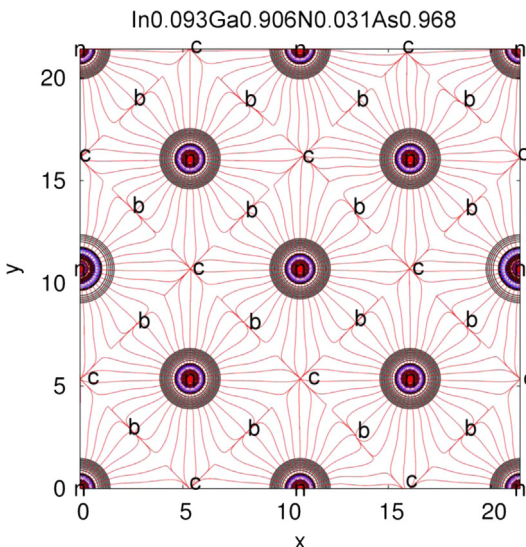


Fig. 8. In red lines, trajectories traced out by electron density gradient vector field (in electron/bohr³) of In_{0.093}Ga_{0.906}N_{0.031}As_{0.968} at the optimal FP-LAPW geometry. The set of trajectories that terminates at each bond critical points (b) defines an interatomic surface. The set of trajectories that originate at the ring critical (c) points define the perimeter of the interatomic surface. The gradient paths associated with the negative eigenvalues at the (n) point terminate at this CP and define the zero-flux surfaces that partition the crystal into unique fragments (the atomic basins).

3.3. Density of states

In order to understand the electronic properties of our quaternary alloys, the electronic density of states (DOS) is defined as the number of allowed states per energy unit. Therefore, we have calculated the density of states (DOS) within the three DFT approximations. Here, we discuss and analyze densities predicted for non-relaxed In_{0.093}Ga_{0.906}As and In_{0.093}Ga_{0.906}N_{0.031}As_{0.968} alloys, using the TB-mBJ approximation. The Fermi level in Fig. 10 is set to zero and indicated by the vertical black dashed line. It can be seen from Fig. 10(b) that the valence band is divided into three sub-bands, the low extends from −15.2 to −14.7 eV, the intermediate between −12.5 and −9.7 eV and the high energy sub-band between −6.5 eV and Fermi level. On decomposing the total DOS into s, p and d states, the low sub-band shows a remarkably strong contribution from the semi-core d-states of Ga and In atoms. The intermediate band region originates from the N_s character, with a small mixture of s states coming from As atoms and In/Ga_s, d orbitals. Near the gap, the higher valence band is divided into two regions. The first, from −6.5 to −3.8 eV, can be attributed to Ga and In_s orbitals and As_p states. The second one between −3.8 eV and the zero energy (E_F) comes mainly from N_p states with a little contribution of Ga/In/As_p. The bottom of the conduction band (CBmin) above the Fermi level is characterized by the band gap energy. Our results reveal that the band gap, according to the TB-mBJ approach, for non relaxed In_{0.093}Ga_{0.906}As and In_{0.08}Ga_{0.92}N_{0.03}As_{0.97} alloys are found to be about 1.382 and 1.26 eV, respectively. The ~3% N incorporated into In_{0.093}Ga_{0.906}As induces a downshift of

Ga_s states towards the Fermi level. The density corresponding to the delocalized s orbitals of Ga atom is the most dominant in the lower region of the conduction band near the Fermi level (0.4 electron/eV). In the DOS calculation for the In_{0.093}Ga_{0.906}N_{0.031}As_{0.968} quaternary alloy the density of state corresponding to the Ga_s orbital overlaps on the density of states of N_s orbital which is a highly localized orbital, leading to a downwards shift in the conduction band minimum and therefore a reduction in the band gap energy.

3.4. Optical properties

The shift of the band gap in the GaInAsN alloys permits technological applications of these compounds directly related to their emission, reflectivity and absorption properties. In fact, III-V semiconductors and III-nitride groups in particular have been recognized as the most promising semiconductor groups for optoelectronics applications, due to the considerable variety of structures that can be tailored to exploit a variety of optoelectronics devices. Among III-nitride materials, InGaNAs alloy plays a fundamental role in developing new devices.

In this part, we will present the optical properties coming into play when a material such as In_xGa_{1-x}N_yAs_{1-y} is subjected to a light beam. These important properties are related to the complex dielectric function $\epsilon(\omega)$ that can be used to describe the linear response crystal of the system to electromagnetic radiation, which is essentially linked to the electronic band structures. The real and the imaginary parts of the dielectric function are, respectively, $\epsilon_1(\omega)$ and $\epsilon_2(\omega)$ [64].

The imaginary part of the dielectric function in the long wavelength limit has been obtained directly from the electronic structure calculation, using the joint density of states and the optical matrix elements. The real part $\epsilon_1(\omega)$ of the dielectric function can be derived from the imaginary part $\epsilon_2(\omega)$ through the Kramers-Kronig relation [65]. From these parts of the dielectric function we deduce the refractive index $n(\omega)$ and the extinction coefficient $k(\omega)$:

$$n(\omega) = \sqrt{\frac{(\epsilon_1(\omega)^2 + \epsilon_2(\omega)^2)^{1/2} + \epsilon_1(\omega)}{2}} \quad (10)$$

$$k(\omega) = \sqrt{\frac{(\epsilon_1(\omega)^2 + \epsilon_2(\omega)^2)^{1/2} - \epsilon_1(\omega)}{2}} \quad (11)$$

Both $n(\omega)$ and $k(\omega)$ can be incorporated into a single quantity called the complex index of refraction $n^*(\omega)$ which can be given by [66]

$$n^*(\omega) = n(\omega) + ik(\omega) = \sqrt{\epsilon(\omega)} = \sqrt{\epsilon_1(\omega) + i\epsilon_2(\omega)} \quad (12)$$

Since all our materials have a cubic symmetry, we need to calculate only one dielectric tensor component to completely characterize the linear optical properties. A dense mesh of uniformly distributed k-points is required in order to calculate $\epsilon_1(\omega)$ with a good representation of $\epsilon_2(\omega)$. Hence the Brillouin Zone (BZ) integration was performed with 172 k-points in the irreducible part of the BZ. The half-width Lorentzian broadening is set to 0.1 eV.

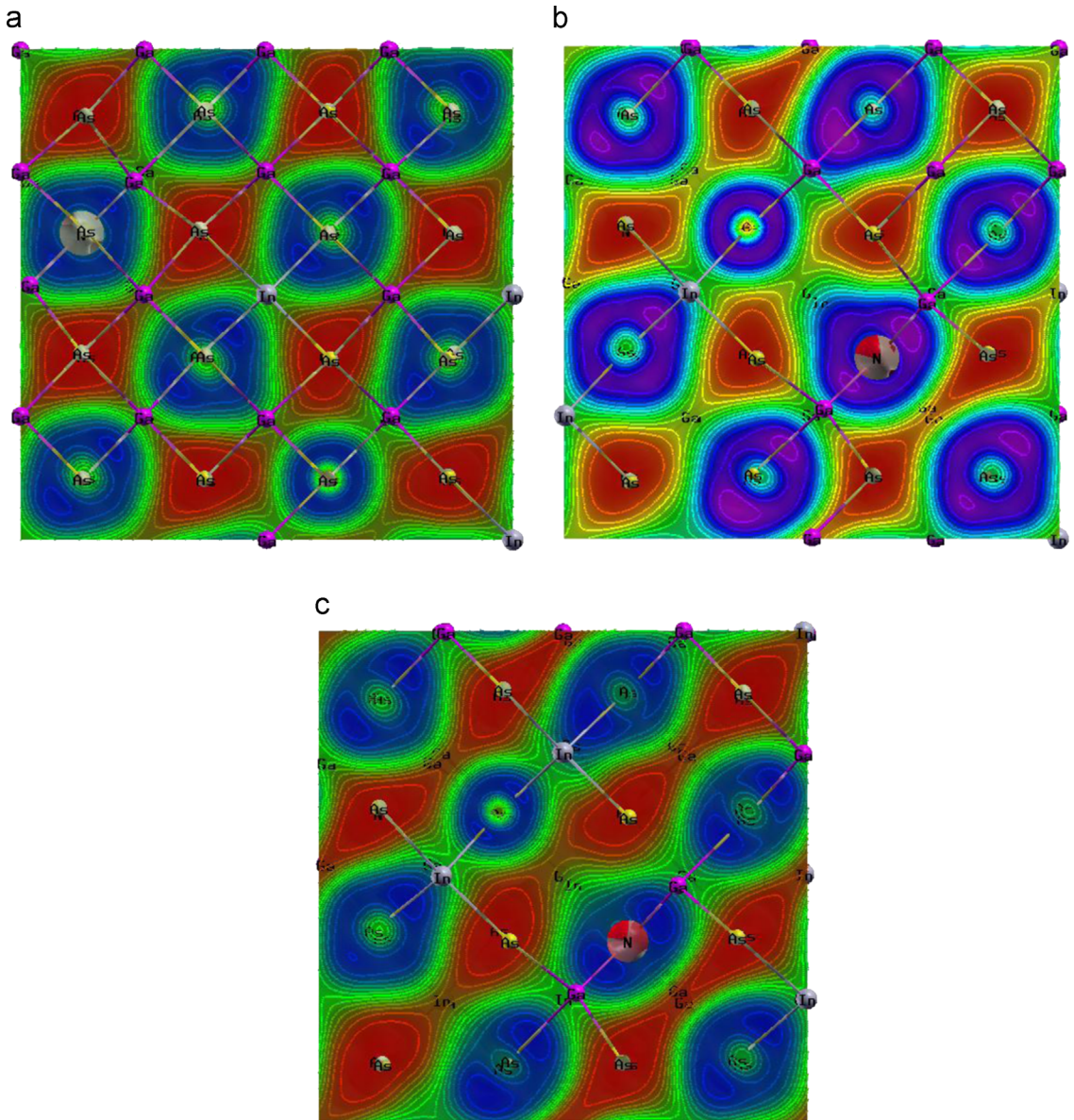


Fig. 9. 2D map of the isovalue surfaces ($\nabla^2\rho_n$) of the different quaternary alloys (a) $\text{In}_{0.093}\text{Ga}_{0.906}\text{N}_{0.031}\text{As}_{0.968}$, (b) $\text{In}_{0.156}\text{Ga}_{0.843}\text{N}_{0.062}\text{As}_{0.937}$ and (c) $\text{In}_{0.25}\text{Ga}_{0.75}\text{N}_{0.093}\text{As}_{0.906}$. The Laplacian is constructed from second partial derivatives, so it is essentially a measure of the curvature of the function in three dimensions. The Laplacian of any scalar field shows where the field is locally concentrated or depleted, and it has a negative value wherever the scalar field is locally concentrated and a positive value where it is locally depleted.

The spectral variations of the dielectric function $\epsilon(\omega)$ for non-relaxed $\text{In}_{0.093}\text{Ga}_{0.906}\text{N}_{0.031}\text{As}_{0.968}$, $\text{In}_{0.156}\text{Ga}_{0.843}\text{N}_{0.062}\text{As}_{0.937}$ and $\text{In}_{0.25}\text{Ga}_{0.75}\text{N}_{0.093}\text{As}_{0.906}$ for a radiation up to 16 eV are shown in Figs. 11 and 12. As can be seen in Fig. 12, the threshold points (here labeled E_0) of the dielectric function $\epsilon(\omega)$ occur at 0.91, 1.21 and 1.27 eV for $\text{In}_{0.25}\text{Ga}_{0.75}\text{N}_{0.093}\text{As}_{0.906}$, $\text{In}_{0.156}\text{Ga}_{0.843}\text{N}_{0.062}\text{As}_{0.937}$, $\text{In}_{0.093}\text{Ga}_{0.906}\text{N}_{0.031}\text{As}_{0.968}$, respectively. In most instances, these critical points ($\Gamma_{15v}-\Gamma_{1c}$) are usually related to the energy band gap of material which corresponds to direct optical transitions (inter-band process) from the highest valence and the lowest conduction band i.e. the occupied states below the Fermi level and the unoccupied states in a higher band. The absorption threshold increases

with decreasing x and y concentrations, which is consistent with the increases in direct band gap. The corresponding numeric values of these peaks for all three materials are summarized in Table 5. Beyond these points, the curve increases rapidly. As a general observation, all curves of Fig. 12 show two major peaks in our calculations; the first major peaks (labeled E_1) move to lower energies and peak heights reduce with increase of In and N compositions.

The second ones, labeled E_2 , shift towards higher energies and peak heights reduce with increase of x and y compositions. The most important contribution to these peaks corresponds to the electronic transition between

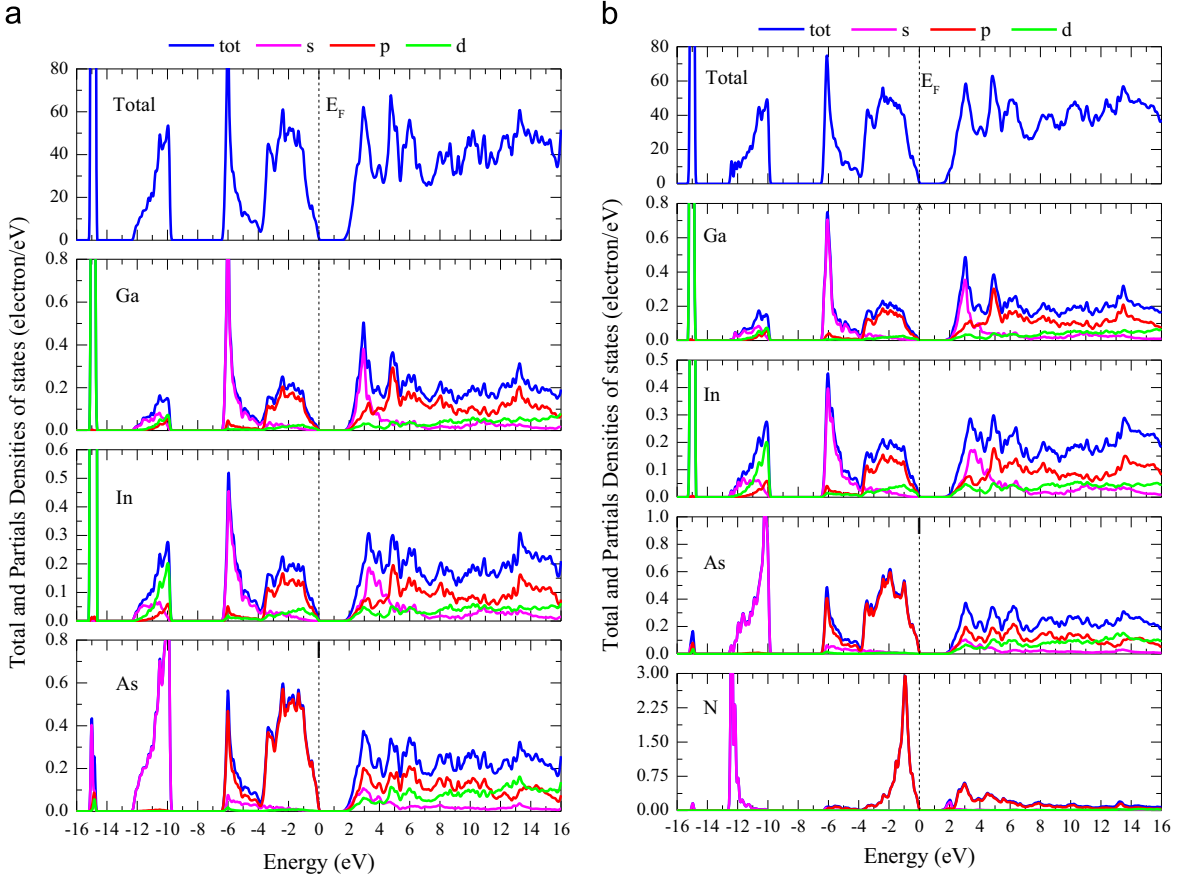


Fig. 10. Total and Partial density of states calculated for (a) $\text{In}_{0.093}\text{Ga}_{0.906}\text{As}$ and (b) for $\text{In}_{0.093}\text{Ga}_{0.906}\text{N}_{0.031}\text{As}_{0.968}$ using the modified Becke-Johnson method.

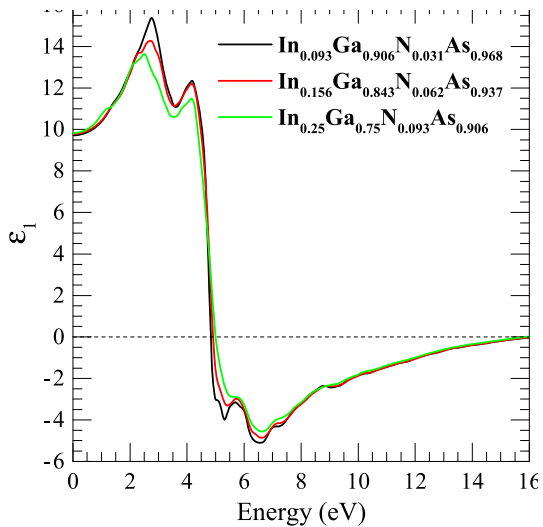


Fig. 11. $\epsilon_1(E)$ spectra for no relaxed $\text{In}_{0.093}\text{Ga}_{0.906}\text{N}_{0.031}\text{As}_{0.968}$, $\text{In}_{0.156}\text{Ga}_{0.843}\text{N}_{0.062}\text{As}_{0.937}$ and $\text{In}_{0.25}\text{Ga}_{0.75}\text{N}_{0.093}\text{As}_{0.906}$ alloys using the modified Becke-Johnson approach (TB-mBJ).

occupied Ga(As)*s/p* and N*p* states and unoccupied Ga(N)*s/p* and As*s/p/d* states along R, Γ and X direction in the Brillouin Zone (BZ).

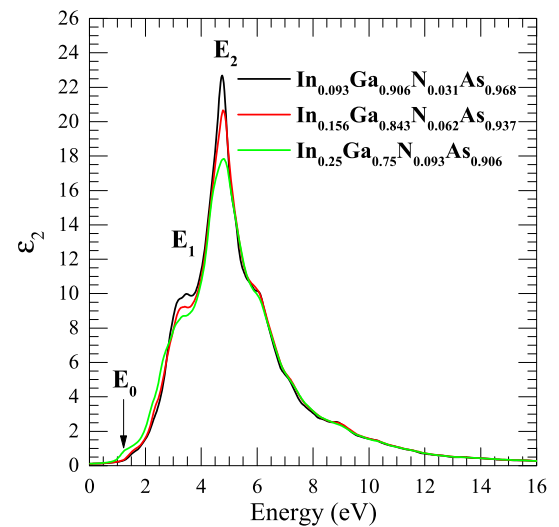


Fig. 12. $\epsilon_2(E)$ spectra for no relaxed $\text{In}_{0.093}\text{Ga}_{0.906}\text{N}_{0.031}\text{As}_{0.968}$, $\text{In}_{0.156}\text{Ga}_{0.843}\text{N}_{0.062}\text{As}_{0.937}$ and $\text{In}_{0.25}\text{Ga}_{0.75}\text{N}_{0.093}\text{As}_{0.906}$ alloy using the modified Becke-Johnson approach (TB-mBJ).

The TB-mBJ results of $\epsilon_1(\omega)$ for all materials without relaxation effect are shown in Fig. 11. The limiting value of the real part of complex dielectric function obtained at a

Table 5

The critical points (in eV) of $\epsilon_2(E)$, static dielectric constant, static refractive index and static reflectivity for $\text{In}_x\text{Ga}_{1-x}\text{N}_y\text{As}_{1-y}$ within TB-mBJ approximation.

Materials	Critical points			$\epsilon_1(0)$	$n(0)$	$R(0)$
	E_0	E_1	E_2			
$\text{In}_{0.093}\text{Ga}_{0.906}\text{N}_{0.031}\text{As}_{0.968}$	1.27	3.48	4.74	9.72	3.11	26.44
$\text{In}_{0.156}\text{Ga}_{0.843}\text{N}_{0.062}\text{As}_{0.937}$	1.21	3.42	4.78	9.78	3.12	26.58
$\text{In}_{0.25}\text{Ga}_{0.75}\text{N}_{0.093}\text{As}_{0.906}$	0.91	3.34	4.80	9.83	3.13	26.65

frequency of irradiation approaching zero is called static dielectric constant $\epsilon_1(0)$. Our calculated values of $\epsilon_1(0)$ found in this way are 9.72, 9.78 and 9.83 for $(x,y)=(3\% \text{ and } 1\%)$, $(5\% \text{ and } 2\%)$, and $(8\% \text{ and } 3\%)$, respectively. The calculated static dielectric constant $\epsilon_1(0)$ increases with increasing concentration of x and y , which is consistent with the decrease of the direct band gap value, indicating that the obtained $\epsilon_1(0)$ is in inverse relationship with band gap accorded to the Penn model [67].

The calculated real and imaginary parts of the complex index $n^*(\omega)$ of un-relaxed quaternary alloys are, respectively, displayed in Figs. 13 and 14 over a range of photon energies up to 16 eV. The refractive index is defined by M. Fox [68] as the ratio of the quantities of light in vacuum to those in the considered matter.

The calculated zero refractive indices of $\text{In}_x\text{Ga}_{1-x}\text{N}_y\text{As}_{1-y}$ for three composition alloys are presented in Table 5. The spectral plots of the refractive index of Fig. 13 show two main peaks. The first highest peak occurs at 2.82 for $\text{In}_{0.093}\text{Ga}_{0.906}\text{N}_{0.031}\text{As}_{0.968}$ quaternary alloy. By increasing x and y compositions the first peak moves to 2.76 and 2.54 eV for $\text{In}_{0.156}\text{Ga}_{0.843}\text{N}_{0.062}\text{As}_{0.937}$ and $\text{In}_{0.25}\text{Ga}_{0.75}\text{N}_{0.093}\text{As}_{0.906}$ and its height decreases by 3.5% and 6%, respectively. The second peaks were found at 4.54, 4.34 and 4.25 eV of photon energy for $(x,y)=(3\% \text{ and } 1\%)$, $(5\% \text{ and } 2\%)$, and $(8\% \text{ and } 3\%)$, respectively. For all three considered materials, the refractive index reaches a maximum value in the visible light region. The calculated extinction coefficients are depicted in Fig. 14. We find three peaks due to the shift of electrons from valence band (VB) to conduction band (CB). The maximum values of extinction coefficient $k(\omega)$ are 3.32, 3.13 and 2.89 at 4.87, 4.94 and 5.03 eV for the three compounds of compositions $(x=3/32, y=1/32)$, $(x=5/32, y=2/32)$ and $(x=8/32, y=3/32)$, respectively.

Reflectivity of light is one of the most important parameters in optical calculations. In fact, reflectivity is sensitive to a complicated combination of $\epsilon_1(\omega)$ and $\epsilon_2(\omega)$. This is usually described by the reflection light energy part at the surface of a semiconductor. We plot the reflectivity $R(\omega)$ calculated without relaxation effect within TB-mBJ functional as a function of photon energy in Fig. 15. The zero frequency reflectivities are 26.4%, 26.5% and 26.6% for $\text{In}_{0.25}\text{Ga}_{0.75}\text{N}_{0.093}\text{As}_{0.906}$, $\text{In}_{0.156}\text{Ga}_{0.843}\text{N}_{0.062}\text{As}_{0.937}$, $\text{In}_{0.093}\text{Ga}_{0.906}\text{N}_{0.031}\text{As}_{0.968}$, respectively.

It is obvious from Fig. 15 that with the addition of In and N, the static reflectivity (reflectivity at 0 eV) increases. The maximum values presented are 57.7%, 56.5% and 55.2% located at about 7.42, 7.52 and 7.59 eV of photon energy, for concentration x and y of $(3\% \text{ and } 1\%)$, $(5\% \text{ and } 2\%)$, and $(8\% \text{ and } 3\%)$, respectively. With increasing indium and

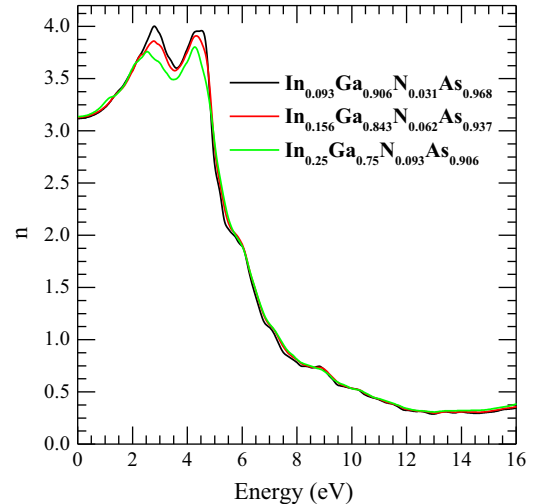


Fig. 13. Refractive index $n(E)$ for no relaxed $\text{In}_{0.093}\text{Ga}_{0.906}\text{N}_{0.031}\text{As}_{0.968}$, $\text{In}_{0.156}\text{Ga}_{0.843}\text{N}_{0.062}\text{As}_{0.937}$ and $\text{In}_{0.25}\text{Ga}_{0.75}\text{N}_{0.093}\text{As}_{0.906}$ alloys using the modified Becke-Johnson approach.

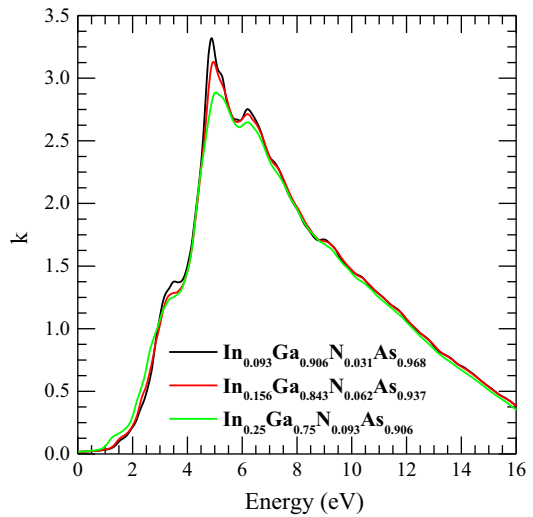


Fig. 14. Extinction coefficient $k(E)$ for no relaxed $\text{In}_{0.093}\text{Ga}_{0.906}\text{N}_{0.031}\text{As}_{0.968}$, $\text{In}_{0.156}\text{Ga}_{0.843}\text{N}_{0.062}\text{As}_{0.937}$ and $\text{In}_{0.25}\text{Ga}_{0.75}\text{N}_{0.093}\text{As}_{0.906}$ alloys using the modified Becke-Johnson approach.

nitrogen concentrations, the reflectivity maximum shifts towards high excitations. The wavelength of the reflectivity maximum is found around $0.164 \mu\text{m}$ ($\sim 164 \text{ nm}$).

The light absorption is quantified by the absorption coefficient α [68]. The latter is calculated, as a function of

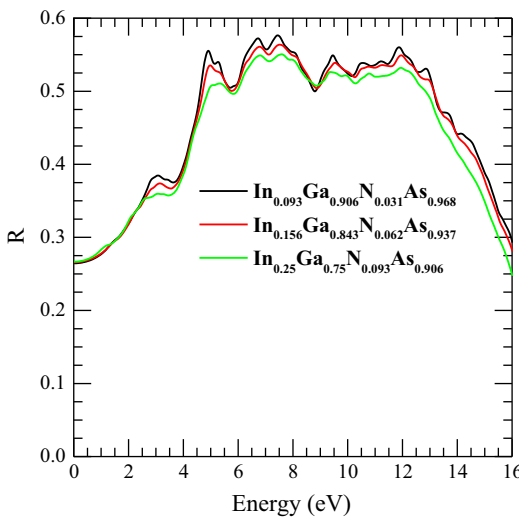


Fig. 15. The calculated spectra reflectivity $R(E)$ versus photon energy of InGaNAs without relaxation by using the modified Becke-Johnson approach.

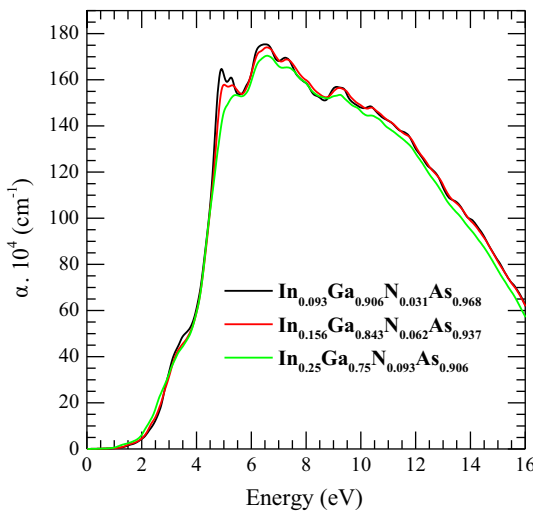


Fig. 16. Absorption coefficient as function of photon energy of InGaNAs without relaxation by using the modified Becke-Johnson approach.

photon energy, from the average values of the index of the absorption $k(\omega)$. The results for all three non-relaxed materials are plotted in Fig. 16, where a zero absorption coefficient for all materials is observed for photons possessing energies below the band gap in the infrared region (at the longer wavelengths ~ 1200 nm). The absorption coefficient is very low in the visible region at optimum wavelength (from 680 to 390 nm), and reaches its maximum value at short wavelength in the ultraviolet region (≤ 380 nm); after that the latter drops sharply at high energies. The onset of the absorption is called by M. Fox [68] as the fundamental absorption edge. This quantity shifts to higher energies with decreasing indium (In) and nitrogen (N) contents. The calculation results in Fig. 16 indicate the usefulness of these quaternary alloys for

absorption purposes in the ultraviolet-C region of the electromagnetic spectrum.

4. Conclusion

In summary, our calculations aim to study the structural, electronic and optical properties of $\text{In}_x\text{Ga}_{1-x}\text{N}_y\text{As}_{1-y}$ quaternary alloy using the FP-LAPW method. We have firstly investigated the structural parameters of the binary compounds GaAs, InAs, GaN and InN. The results are in agreement with the experimental values and other multi reference data. Secondly, the equilibrium structural properties from volume optimization for the quaternary $\text{In}_x\text{Ga}_{1-x}\text{N}_y\text{As}_{1-y}$ semiconductor alloys were obtained and discussed. The calculated lattice matching expression for quaternary $\text{In}_x\text{Ga}_{1-x}\text{N}_y\text{As}_{1-y}$ on the GaAs substrate was determined. The incorporation of one Nitrogen atom into host semiconductor such as $\text{In}_{0.093}\text{Ga}_{0.906}\text{As}$ leads to a decrease in the lattice parameter. In addition to BAC model, the band gap energy has been investigated within the three exchange approximations with and without the atomic relaxation. By increasing the x and y concentration, we observed a decrease of the band gap in the quaternary alloys. This is due to the strong interaction between the extended states of the conduction band of the host semiconductor and the localized resonant states of the nitrogen N. We have paid special attention to the effect of geometrical relaxation that strongly affects the band gap. The relaxation is very localized about the Nitrogen substituted site and primarily involves motion of the two adjacent atoms to the substituted lattice site. To estimate the error made by the three DFT approximations to the energy gap, we can build on the band anti-crossing model (BAC). This model calculation allows us to obtain very accurate results, with a good estimate of the error bars calculated for low Nitrogen contents. In the other hand, a good improvement has been found with TB-mBJ approach compared to those with WC-GGA and EV-GGA in the estimation of the band gap. The materials which have bandgaps less than 1.3 eV are used for Near-Infrared light devices.

The total and partial densities of state for $\text{In}_x\text{Ga}_{1-x}\text{N}_y\text{As}_{1-y}$ at $x=3/32$ and $y=1/32$ have been calculated within the TB-mBJ approximation. The analysis of the PDOS shows that the incorporation of $\sim 3\%$ N into $\text{In}_{0.093}\text{Ga}_{0.906}\text{As}$ induces a downshift of Ga_s states towards the Fermi level. We have also presented results (without relaxation) for the real and imaginary parts of dielectric function. From the real and imaginary parts of the dielectric function, the reflectivity, the refractive index and the absorption coefficient were obtained and discussed in details in order to collect much information of these alloys of great number of possible applications for optoelectronics devices.

Acknowledgments

The authors thank Pr. Aissat Abdelkader (University of Blida) for many useful discussions.

Parts of this investigation have been done in the Laboratoire de physique théorique Tlemcen.

References

- [1] F. Alexandre, Dilute Nitride Semiconductors, M. Henini Edition, Chapter 2, Epitaxial Growth of Dilute Nitrides by Metal–Organic Vapour Phase Epitaxy, Elsevier, 2005.
- [2] K. Uesugi, I. Suemune, Jpn. J. Appl. Phys. 36 (1997) 1572–1575.
- [3] J.N. Baillargeon, K.Y. Cheng, G.E. Hofer, P.J. Pearah, K.C. Hsieh, Appl. Phys. Lett. 60 (1992) 2540–2542.
- [4] W. Shan, W. Walukiewicz, K.M. Yu, J. Wu, J.W. Ager, E.E. Haller, H.P. Xin, C.W. Tu, Appl. Phys. Lett. 76 (2000) 3251–3253.
- [5] W.G. Bi, C.W. Tu, J. Appl. Phys. 80 (1996) 1934–1936.
- [6] W. Shan, K.M. Yu, W. Walukiewicz, J.W. Ager, E.E. Haller, M.C. Ridgway, Appl. Phys. Lett. 75 (1999) 1410–1412.
- [7] W. Shan, W. Walukiewicz, K.M. Yu, J.W. Ager, E.E. Haller, J.F. Geisz, D. J. Friedman, J.M. Olson, S.R. Kurtz, C. Nauka, Phys. Rev. B 62 (2000) 4211–4214.
- [8] J. Wagner, T. Geppert, K. Kohler, P. Ganser, M. Maier, Appl. Phys. Lett. 83 (2003) 2799–2801.
- [9] V.A. Elyukhin, L.P. Sorokina, S.A. Nikishin, Crystal Growth & Design 4 (2) (2004) 337–341.
- [10] J.O. Maclean, Dilute Nitride Semiconductors, M. Henini Edition, Chapter 3, The Chemical Beam Epitaxy of Dilute Nitride Alloy Semiconductors, Elsevier, 2005.
- [11] M. Kondow, K. Uomi, A. Niwa, T. Kitatani, S. Watahiki, Y. Yazawa, Jpn. J. Appl. Phys., Part 1 35 (1996) 1273–1275.
- [12] K.M. Yu, W. Walukiewicz, J. Wu, J.W. Beeman, J.W. Ager, E.E. Haller, W. Shan, H.P. Xin, C.W. Tu, M.C. Ridgway, J. Appl. Phys. 90 (2001) 2227–2234.
- [13] S. Procz, M. Fiederle, M. Kunzer, K. Köhler, J. Wagner, J. Appl. Phys. 103 (2008) 073103.
- [14] E. Gallardo, S. Lazić, J.M. Calleja, J. Miguel-Sánchez, M. Montes, A. Hierro, R. Gargallo-Caballero, A. Guzman, E. Munoz, A.M. Tweldeberhan, S. Fahy, Physica E 40 (2008) 2084–2086.
- [15] S. Lazić, J.M. Calleja, R. Hey, K. Ploog, phys. stat. sol. (b) 243 (7) (2006) 1634–1638.
- [16] G. Steinle, H. Riechert, A. Yu Egorov, Electronics Letters 34 (2) (2001) 93–95.
- [17] J.M. Ulloa, A. Hierro, J. Miguel-Sánchez, A. Guzmán, E. Touriné, J.L. Sanchez-Rojas, E. Calleja, Appl. Phys. Lett. 85 (2004) 40–42.
- [18] T. Kitatani, K. Nakahara, M. Kondow, K. Uomi, T. Tanaka, Jpn. J. Appl. Phys. 39 (2000) L86.
- [19] K. Kassali, N. Bouarissa, Microelectronic Engineering 54 (2000) 277–286.
- [20] J.B. Heroux, X. Yang, W.I. Wang, Appl. Phys. Lett. 75 (1999) 2716–2718.
- [21] G.S. Kinsey, D.W. Gotthold, A.L. Holmes Jr., et J.C. Campbell, Appl. Phys. Lett. 77 (2000) 1543–1544.
- [22] N.Y. Li, P.C. Chang, A.G. Baca, X.M. Xiue, P.R. Sharp, H.Q. Hou, Electronics Letters 36 (1) (2000) 81–83.
- [23] D.J. Friedman, J.F. Geisz, S.R. Kurtz, J.M. Olson, Journal of Crystal Growth 195 (1998) 409–415.
- [24] L.F. Bian, D.S. Jiang, P.H. Tan, S.L. Lu, B.Q. Sun, L.H. Li, J.C. Harmand, Solid State Communications 132 (2004) 707–711.
- [25] Y. Sun, A. Erol, M. Yilmaz, M.C. Arikhan, B. Ulug, A. Ulug, N. Balkan, M. Sopanen, O. Reenttilä, M. Mattila, C. Fontaine, A. Arnoult, Opt Quant Electron 40 (2008) 467–474.
- [26] S.R. Kurtz, A.A. Allerman, E.D. Jones, J.M. Gee, J.J. Banas, B. E. Hammons, Appl. Phys. Lett. 74 (1999) 729–731.
- [27] M. Aslan, B.G. Yalçın, M. Ustundag, Journal of Alloys and Compounds 519 (2012) 55–59.
- [28] P. Blaha, K. Schwarz, G.H. Madsen, D. Kvasnicka, J. Luitz, FP-L/APW+lo Program for Calculating Crystal Properties, K. Schwarz, Techn. WIEN2K, Austria (2001).
- [29] W. Kohn, L.J. Sham, Phys. Rev 140 (1965) 1133.
- [30] Z. Wu, R.E. Cohen, Phys. Rev. B. 73 (2006) 235116.
- [31] P. Dufek, P. Blaha, K. Schwarz, Phys. Rev. B 50 (1994) 7279–7283.
- [32] E. Engel, S.H. Vosko, Phys. Rev. B 47 (1993) 13164.
- [33] F. Tran, P. Blaha, Phys. Rev. Lett. 102 (2009) 226401.
- [34] O. Madelung (Ed.), Semiconductors, Group IV Elements and III–V Compounds, Landolt–Bornstein, New Series, Group III, vol. 17, Pt. a, Springer, Berlin, 1991.
- [35] H. Morkoç, Handbook of Nitride Semiconductors and Divices, volum. 1, WILEY-VCH Verlag GmbH & Co. KGaA, 2008.
- [36] J.R. Mullhäuser, B. Jenichen, M. Wassermeier, O. Brandt, K.H. Ploog, Appl. Phys. Lett. 71 (1997) 909.
- [37] F.D. Murnaghan, Proc. Natl. Acad. Sci. Usa 30 (1944) 244–247.
- [38] A. Alkauskas, P. Deák, J. Neugebauer, A. Pasquarello, C.G. Van de Walle, Advanced Calculations for Defects in Materials: Electronic Structure Methods, First Edition, WILEY-VCH Verlag GmbH & Co. KGaA, 2011.
- [39] L. Vegard, Z. Phys 5 (1921) 17–26.
- [40] R. Enderlein, N.J.M. Horing, Fundamentals of Semiconductor Physics and Devices, World Scientific Publishing Co.Pte.Ltd, 1997.
- [41] B. Merabet, H. Abid, N. Sekkal, Physica B 406 (2011) 930–935.
- [42] F. El Haj Hassan, A.V. Postnikov, O. Pagès, Journal of Alloys and Compounds 504 (2010) 559–565.
- [43] H. Shi, Y. Duan, Physics Letters A 373 (2008) 165–168.
- [44] K.H. Hellwege, O. Madelung, Landolt-Bornstein, Semiconductors Physics of Group IV Elements and III–V Alloys, New Series, Group III, (1982).
- [45] P. Rinke, M. Winkelkemper, A. Qteish, D. Bimberg, J. Neugebauer, M. Scheffler, Phys. Rev. B 77 (2008) 075202.
- [46] I. Vurgaftman, J.R. Meyer, L.R. Ram-Mohan, J. Appl. Phys. 89 (2001) 5815.
- [47] J. Serrano, A. Rubio, E. Hernandez, A. Munoz, A. Mujica, Phys. Rev. B 62 (2000) 16612–16623.
- [48] Z. Feng, H. Hu, S. Cui, W. Wang, C. Lu, Cent. Eur. J. Phys. 7 (4) (2009) 786–790.
- [49] J. Kim, M.V. Fischetti, Appl. Phys. J 108 (2010) 013710.
- [50] R. Ahmed, S.J. Hashemifar, H. Akbarzadeh, M. Ahmed, F. e-Aleem, Computational Materials Science 39 (2007) 580–586.
- [51] M. Seifikar, E.P. O'Reilly, S. Fahy, phys. stat. sol. (b) 248 (5) (2011) 1176–1179.
- [52] W. Shan, W. Walukiewicz, J.W. Ager, E.E. Haller, J.F. Geisz, D.J. Friedman, J.M. Olson, S.R. Kurtz, Phys. Rev. Lett. 82 (1999) 1221–1224.
- [53] I. Vurgaftman, J.R. Meyer, J. Appl. Phys. 94 (2003) 3675–3696.
- [54] C. Skierbiszewski, Semicond. Sci. Technol. 17 (2002) 803–814.
- [55] A. Aissat, S. Nacer, M. Bensebti, J.P. Vilcot, Microelectronics Journal 40 (2009) 10–14.
- [56] M.I. Ziane, Z. Bensaad, T. Ouahrani, B. Labdelli, H. Bennacer, H. Abid, Materials Science in Semiconductor Processing 16 (2013) 1138–1147.
- [57] H. Jiang, J. Chem. Phys. 138 (2013) 134115.
- [58] R. Ahmed, H. Akbarzadeh, F. e-Aleem, Physica B 370 (2005) 52–60.
- [59] A. Abdiche, H. Abid, R. Riane, A. Bouaza, ACTA PHYSICA POLONICA A 117 (2010) 921–927.
- [60] S. Turcotte, N. Shtinkov, P. Desjardins, R.A. Masut, R. Leonelli, Journal of Semiconductor Science and Technology A 22 (2004) 776.
- [61] J.F. Geisz, D.J. Friedman, J.M. Olson, S.R. Kurtz, B.M. Keyes, Journal of Crystal Growth 195 (1998) 401–408.
- [62] T. Ouahrani, Eur. Phys. J. B 86 (2013) 369.
- [63] C. Skierbiszewski, I. Gorczyca, S.P. Lepkowski, J. Lusakowski, J. Borysiuk, J. Toivonen, Semicond. Sci. Technol. 19 (2004) 1189.
- [64] S. Adachi, Properties of Semiconductor Alloys: Group-IV, III–V and II–VI Semiconductors, Edit, John Wiley & Sons, Ltd., 2009.
- [65] T. Ouahrani, Ali H. Reshak, R. Khenata, B. Amrani, M. Mebrouki, A. Otero-de-la-Roza, V. Luana, Journal of Solid State Chemistry 183 (2010) 46–51.
- [66] C. Amrosch-Draxl, J.O. Sofo, Linear optical properties of solids within the full potential linearized augmented planewave method (2008) 1–34.
- [67] D.R. Penn, Phys. Rev 128 (1962) 2093.
- [68] Mark Fox, Optical Properties of Solids, Oxford University Press, 2001.